Carpathian Journal of Earth and Environmental Sciences, August 2016, Vol. 11, No 2, p. 547 - 564

CHEMICAL COMPOSITION OF PHLOGOPITE, TOURMALINE AND ILLITE FROM HYDROTHERMAL ALTERATIONS OF THE NISTRU DEPOSIT, BAIA MARE, ROMANIA

Ivan A. BAKSHEEV[1], Floarea DAMIAN[2], Gheorghe DAMIAN[2], Vsevolod Yu. PROKOFIEV[3], Igor' A. BRYZGALOV[1] & Lubov' I. MARUSHCHENKO[1]

[1]Department of Geology, Moscow State University, Leninskie Gory, Moscow 119991, Russia, e-mail: baksheev@geol.msu.ru

[2]Technical University of Cluj Napoca, North University Center of Baia Mare, Romania, 62A Dr. Victor Babeş Street, 430083 Baia Mare, Romania, e-mail: damgeo@cunbm.utcluj.ro & loricadamian@cunbm.utcluj.ro

[3]Institute of Geology of Ore Deposits, Petrography, Mineralogy, and Geochemistry, Russian Academy of Sciences, Staromonetny per. 35, Moscow 119017, Russia, e-mail: vpr@igem.ru

Abstract: The chemical composition of phlogopite, tourmaline, and illite from altered rocks of the Nistru Cu-Au-Bi deposit has been examined. Phlogopite of potassic alteration is enriched in fluorine and is similar in chemical composition to phlogopite from potassic alteration at porphyry copper deposits. Tourmaline occurs as three generations. The first-generation tourmaline is classified as dravite or oxy-dravite; second generation is dravite or schorl; and third generation is classified as dravite. Tourmaline II is enriched in ferric iron. The chemical substitutions in tourmaline I are $Al + O^{2-} \rightarrow Mg^{2+} + OH^{-}$ and $Fe \rightarrow Mg$; in tourmaline II, the substitution is $Fe \rightarrow Mg$; and in tourmaline III, assumed substitution is $Ca + Mg + Fe^{2+} \rightarrow 2Al$ + X-site vacancy. Tourmaline I could crystallize with potassium feldspar in potassic alteration; tourmaline II enriched in ferric iron and tourmaline III are found from propylitic alteration that is not related to porphyry system. Illite corresponds in composition to that of epithermal volcanogenic Au-Ag deposits. Thus, the chemical composition of examined minerals indicates three different hydrothermal stages at the Nistru deposit: (1) early porphyry not mentioned so far, (2) later propylitic accompanying minor ore mineralization and not related to porphyry system and (3) epithermal volcanogenic accompanying the base and precious metal mineralization.

Key words: phlogopite, tourmaline, illite, Baia Mare, Nistru, chemical composition, porphyry-epithermal system.

1. INTRODUCTION

The Nistru deposit is referred to the low-sulfidation type of epithermal systems (Marcoux et al., 2002). According to (Sillitoe & Hedenquist, 2003) any type of epithermal deposits, e.g. high-, intermediate, and low-sulfidation, (HS, IS, LS) could be the upper part of a porphyry-epithermal system. The mineralogy and zoning of hydrothermal alterations at the epithermal Nistru deposit is reported in (Damian, 2003). Although no evidences were published so far indicating that Nistru is a part of a porphyry-type system, we identified potassic, propylitic, phyllic, and intermediate argillic alterations, which are typical of porphyry-epithermal systems elsewhere.

The characteristic mineral of potassic alteration is phlogopite. The contents of F and Cl reflect the fugacities of HF and HCl during the formation of potassic alteration (Munoz, 1984; Boomeri et al., 2009, 2010; Selby & Nesbitt, 2000). The Mg and Ti contents allow distinguishing magmatic, re-equilibrated and hydrothermal phlogopite of porphyry deposits (Nachit et al., 2005).

Tourmaline has been described within them propylitic, quartz-sericite (phyllic) and advanced argillic alterations (e.g. Baksheev et al., 2010,

2012b, 2012c; Voudouris, 2014; Lynch & Ortega, 1997; Yavuz et al., 1999). According to Baksheev et al., (2012c), tourmaline from propylitic alteration is characterized by the higher Fe^{3+}/Fe_{tot} value as compared with tourmaline from quartz-sericite alteration that indicates higher fO_2 during the formation of propylitic alteration. Marushchenko et al., (2015) reported low-Ca tourmaline from the quartz-sericite-dolomite alteration adjacent base-metal-bearing veins at the Peschanka and Nakhodka porphyry deposits, Chukchi Peninsula, Russia. They related the low Ca content in the tourmalines to the high fCO_2 resulting in the carbonate precipitation. At the same time, tourmaline from carbonate-free quartz-sericite alteration accompanying copper mineralization is characterized high Ca content, (Marushchenko et al., 2015). Tourmalines from advanced argillic alteration trend towards vacancy-rich compositions (Collins, 2010). This is caused by the low pH value of mineralizing fluids.

Layered silicates are characteristic minerals of quartz-sericite and various argillic alterations. For example, pyrophyllite is common in advanced argillic alteration; muscovite and phengite are found quartz-sericite rock. Small amount of Illite is found in quartz-sericite alteration, where it replaces muscovite or phengite. In the intermediate argillic alteration, where this mineral is major, it is associated with smectite and kaolinite, (Parry & Jusumback, 2000). Illite is not typical of advance argillic alteration. Therefore illite is a key mineral for transition from quartz-sericite to intermediate argillic alteration.

This study examines for the first time the chemical composition of phlogopite, tourmaline, and illite from types of alterations at the Nistru deposit and suggests that this deposit is a part of porphyry-epithermal system. In addition, the chemical composition of various tourmaline generations has been used to identify distinct hydrothermal stages within the deposit.

2. GENERAL GEOLOGY AND MINERALOGY

The metallogenetic activity in the Baia Mare area is related to the Neogene magmatism in the southern part of the Gutîi Mountains, north-western Romania (Fig. 1A). The calc-alkaline magmatism, (Pécskay et al., 1995, Mason et al., 1998, Harangi et al., 2006, Seghedi et al., 2005) is related to the Neogene subduction formed as resulted of collision of south-eastern border of the East-European Platform and Alcapa and Tisia lithospheric blocks, Seghedi et al., 2004.

The Nistru deposit is located in the western part of the Baia Mare metallogenetic district and in the southern part of the volcanic area of Gutîi Mountains. The volcanic area comprises abundant Sarmatian pyroxene andesite with minor Pannonian quartz andesites in the northern and south-eastern part (Fig. 1A). The oldest rocks belonging to the explosive phase of the volcanic activity in the area are Badenian pyroclastic rocks (Borcoş et al., 1972a).

Subvolcanic bodies are spatially related to the volcanic rocks. According to (Borcoş et al., 1972a), the intrusive activity took place after the eruption of pyroxene andesite. The K-Ar age of pyroxene andesite 13.4-12.1Ma, (Edelstein et al., 1992; Pécskay et al., 1994) determined from bulk rock samples overlaps Late Badenian and Early Sarmatian.

According to (Borcoş et al., 1972b), the metallogenetic activity is controlled by the Piatra Handal volcanic edifice with vein clusters on its north-western and eastern sides (Fig. 1A). Piatra Handal is the highest hill in the Nistru area. The Piatra Handal neck (Fig. 1B) is distinguished by brecciated character and intense silicification of rocks with hematite staining. In the deep part of the Nistru area, there is a succession of various subvolcanic bodies (Fig. 1B). On the surface are exposed by erosion in the Nistru Valley (Fig. 1A).

2.1 Intrusive rocks in the Nistru zone

Most subvolcanic bodies of the magmatic intrusive activity in the studied zone, develop in the underground. In the NW of Piatra Handal Hill, (+ 704 m), intrusive rocks do not appear on the surface. These are represented by apophysis in underground mining of 100m below surface. Were distinguished varieties porphyritic of two petrographic types: quartz microdiorite and microdiorite. In the NE, and SE-SW part of Piatra Handal Hill the main intrusion represented by quartz porphyry micro-monzodiorite is to 200m emplaced below surface, (Fig. 1B). This consists of the stock with dimensions, over 1000 m in length between the two major copper-bearing (Nepomuc and Domnisoara veins, (Fig.1B), (Damian et al., 2009). This stock is accompanied by apophysis cropped out in the middle part of the Nistru Valley over a length of approximately 2.5 km (Fig. 1A). Overlaid of the stock of quartz porphyry micro-monzodiorite, underground, were identified the porphyry dikes and sills of microdiorite and microgabbro, respectively, (Damian et al., 2009; Damian, 2000). The stock of quartz porphyry micro-monzodiorite is followed by an intrusive quartz andesite body in south-eastern part, (Fig. 1B).

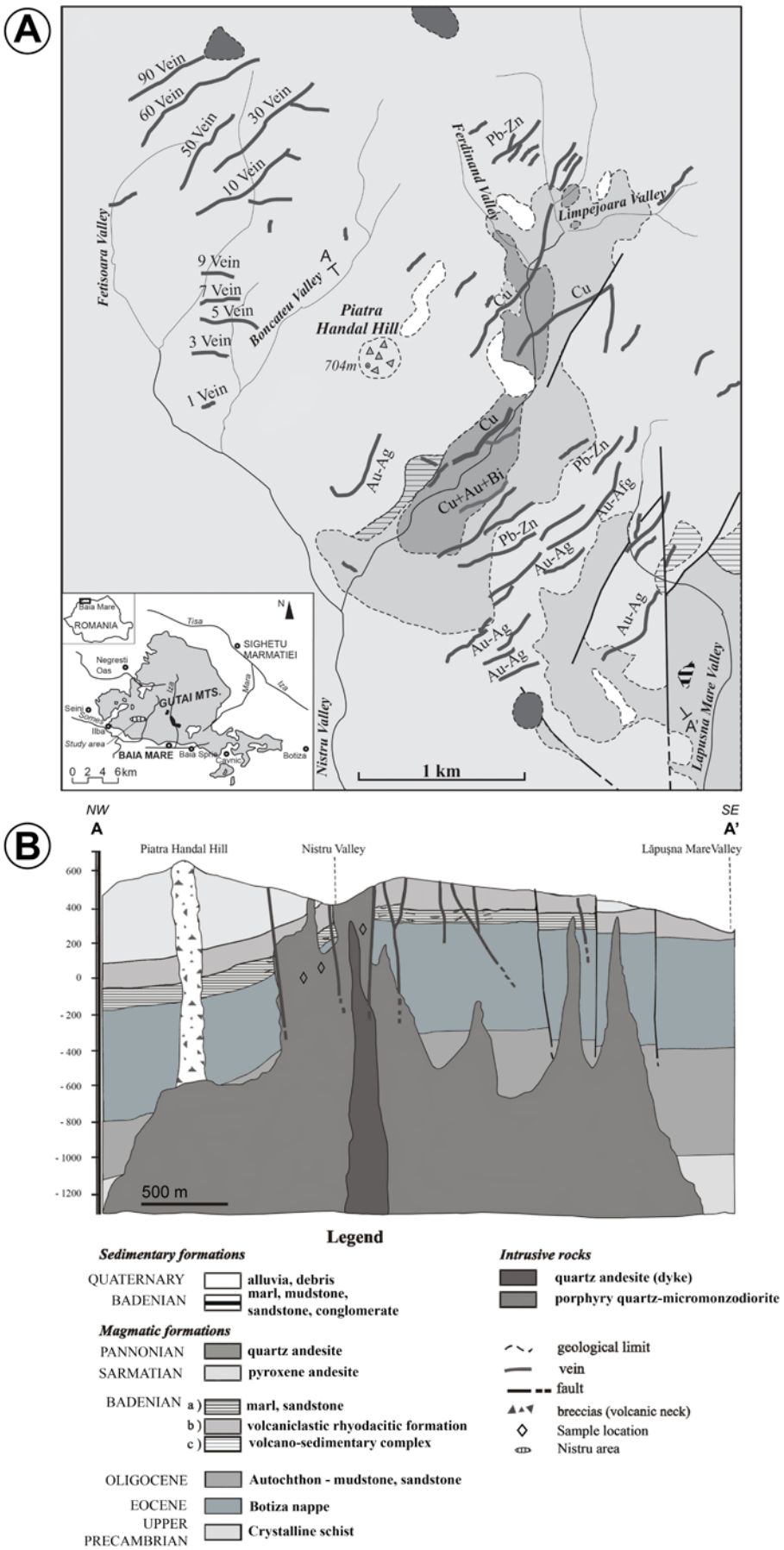

Figure 1. (A) Geological map of the Nistru ore field; (B) NW-SE geological section, modified after Damian et al., (2009).

2.2. Alterations types

The subvolcanic rocks within the Nistru ore field were induced by significant metallogenetic and hydrothermal processes (Damian, 2000; 2003) with hydrothermal alteration zoning comparable with that reported for similar hydrothermal systems elsewhere (Meyer & Hemley, 1967; Pirajno, 1992). The deep level of the central quartz porphyry micro-monzodiorite stock is occupied by a pervasive potassic alteration with potassium feldspar + phlogopite, (Fig. 2c). The potassic zone is contemporaneous and rimmed by propylitic alteration, Fig. 2c) that is extensive in both intrusive and volcanic rocks, (Fig. 2a). Within the quartz porphyry micro-monzodiorite stock, the propylitic alteration is zoned inward from epidote + chlorite- to actinolite-bearing mineral assemblages. Both potassic and propylitic alteration zones are overprinted by phyllic (quartz-sericite) (Fig. 2a, 2b, 2c) and argillic alteration as a result of incursion of the subsequent fluids in the system (Damian, 2003).

Phyllic alteration affects adjacent areas of the copper-bearing veins (Fig. 2c) located at the margins of the quartz porphyry micro-monzodiorite stock and also forms wall-rock alteration of the base-metal-bearing veins, (Fig. 2a). In addition to quartz and muscovite, illite, tourmaline, and pyrite are constituents of this alteration. Intermediate argillic alteration is presented in the upper levels of the Nistru deposit and consists of illite, kaolinite and halloysite.

2.3. The Nistru deposit

The Nistru deposit occupies a surface area of 4-5 km^2 around the Piatra Handal Hill and comprises a series of quartz veins with copper, base-metal and Ag-Au mineralization. These veins are hosted in subvolcanic bodies, pyroxene andesite, and in pyroclastic rocks (Borcoş et al., 1974). In the northwestern part of the Nistru deposit, the ore veins occur in a pyroxene andesite and a subvolcanic quartz porphyry microdiorite at the upper and deeper levels, respectively. The veins at the northeastern and southeastern-southwestern Nistru deposit surround the quartz porphyry micro-monzodiorite stocks and are hosted in quartz porphyry micro-monzodiorite, pyroxene andesite and pyroclastic rocks.

Three ore stages were identified at the Nistru deposit: (1) Cu ± Au and Bi, (2) Pb-Zn, and (3) Au. Mineral assemblages of two first stages are related to the quartz-sericite alteration. Copper ores of the first stage are composed of three successive assemblages: (1) pyrite-chalcopyrite-hematite-quartz-sericite; (2) pyrite-chalcopyrite-quartz, and (3) pyrite-chalcopyrite-native gold-Bi sulfosalts-quartz (Damian, 1999), with subordinate tetradymite (Plotinskaya et al., 2009). The later base-metal mineralization encompasses pyrite--chalcopyrite-sphalerite--galena--native gold--tetrahedrite--Pb sulfosalts assemblage with calcite and quartz as gangue minerals. The third-stage gold mineralization is pyrite-native gold-Ag sulfosalts assemblage with kaolinite and halloysite as gangue minerals.

In the northwestern part of the Nistru deposit all stages of mineralization are telescoped in the same veins, whereas in the northeastern and southeastern-southwestern parts of the Nistru deposit the ore veins are zonally distributed around the subvolcanic stock of quartz-porphyry micro-monzodiorite. A lateral zoning exists, where copper veins hosted in the subvolcanic stock are followed by proximal base-metal veins in near-contact pyroclastic rocks and by distal Ag-Au veins that occur in both pyroxene andesite and pyroclastic rocks.

3. METHODS

The electron microscope study was performed with a JeolJSM–6480LV electron microscope equipped with an Inca Energy-350 EDS and WDS Laboratory of High Spatial Resolution Analytical Techniques at Division of Petrology, Lomonosov Moscow State University. Back-scattered electron (BSE) images were obtained at an accelerating voltage of 15 kV and a current intensity of 14–16nA.

The chemical composition of tourmaline was studied with a CAMEBAX SX–50 electron microprobe, Division of Mineralogy, Lomonosov Moscow State University. An accelerating voltage of 15 kV and a current intensity of 30 nA were used, with a beam diameter of ~3 μm. We used the PAP software for correction procedures, and the following standards: hornblende (Si, Al, Ca, Mg, Fe), orthoclase (K), albite (Na), MgF_2 (F), pyrophanite (Mn, Ti), vanadinite (V), Cr_2O_3 (Cr), and SnO_2 (Sn).

Biotite and illite were examined with an electron microprobe at an accelerating potential 15 kV, a current intensity 15 ± 0.05 nA, and a beam diameter of 3 μm. The ZAF software was used for correction procedures. Profiles of measured elements were optimized and standardized with natural silicates to minimize absolute errors of element measurements in natural and synthetic standard micas.

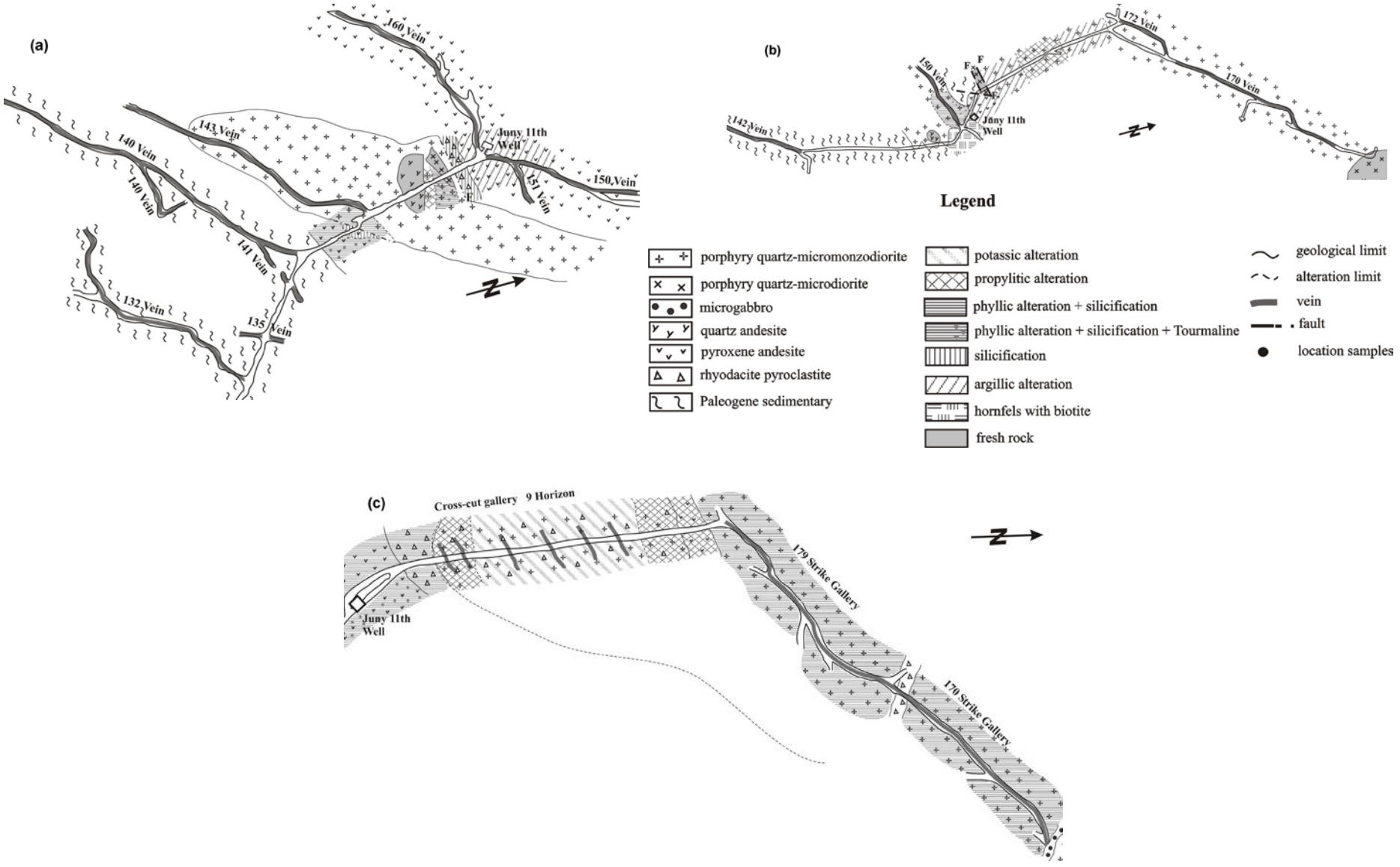

Figure 2. Horizontal distribution of hydrothermal alteration types: +340 level (a); +80 level (b); +25 level (c).

The following standards were used: phengite, phlogopite, MgF_2, muscovite, which were examined with an electron microprobe (Institute of Geology and Mineralogy, Siberian Branch, Russian Academy of Sciences) and bulk-chemical analyses (laboratories of Moscow State Geological Exploration University and Institute of Synthesis of Mineral Raw Materials).

The tourmaline formulae were normalized on the basis of 15 cations exclusive Na, Ca, and K, *i.e.*, assuming no vacancies at the tetrahedral or octahedral sites, and an insignificant content of Li (Henry et al., 2011). Charge-balance constraints were used to estimate the amounts of OH^- and O^{2-} associated with the *V* and *W* anion sites in the structural formula, although there are likely significant uncertainties (Dutrow & Henry, 2000). We further assume that calculated O^{2-} is preferentially incorporated at the *W* site together with F (Henry et al., 2011). The proportion of vacancies (□) was calculated using stoichiometric constraints by means of 1 – (Na + Ca + K). This assumption permits grouping of tourmaline in accordance with the classification proposed by (Henry et al., 2011). The amount of B_2O_3 was calculated from stoichiometric constraints. Due to the lack of material, Fe^{3+} was not estimated by the Mössbauer spectroscopy and in some analyses it was calculated from charge-balance constraints. In the other analyses, Fe is reported as Fe^{2+}. The compositions of phlogopite and illite were normalized on the basis of 22 anions.

4. RESULTS

Phlogopite is a characteristic signature of the potassic altered quartz micro-monzodiorite body. It occurs as brown flakes up to 5 mm in size closely intergrown with potassium feldspar, (Fig. 3a). Phlogopite is F-bearing (0.35-0.54 apfu F); the content of Ti ranges from 2.5 to 4.1 wt. % TiO_2; the $Fe_{tot}/(Fe_{tot}+Mg)$ value varies from 0.12 to 0.21 (Table 1). On the ternary diagram Fe-Ti-Mg (Fig. 4) the compositions fall in the fields of re-equilibrated and hydrothermal biotite.

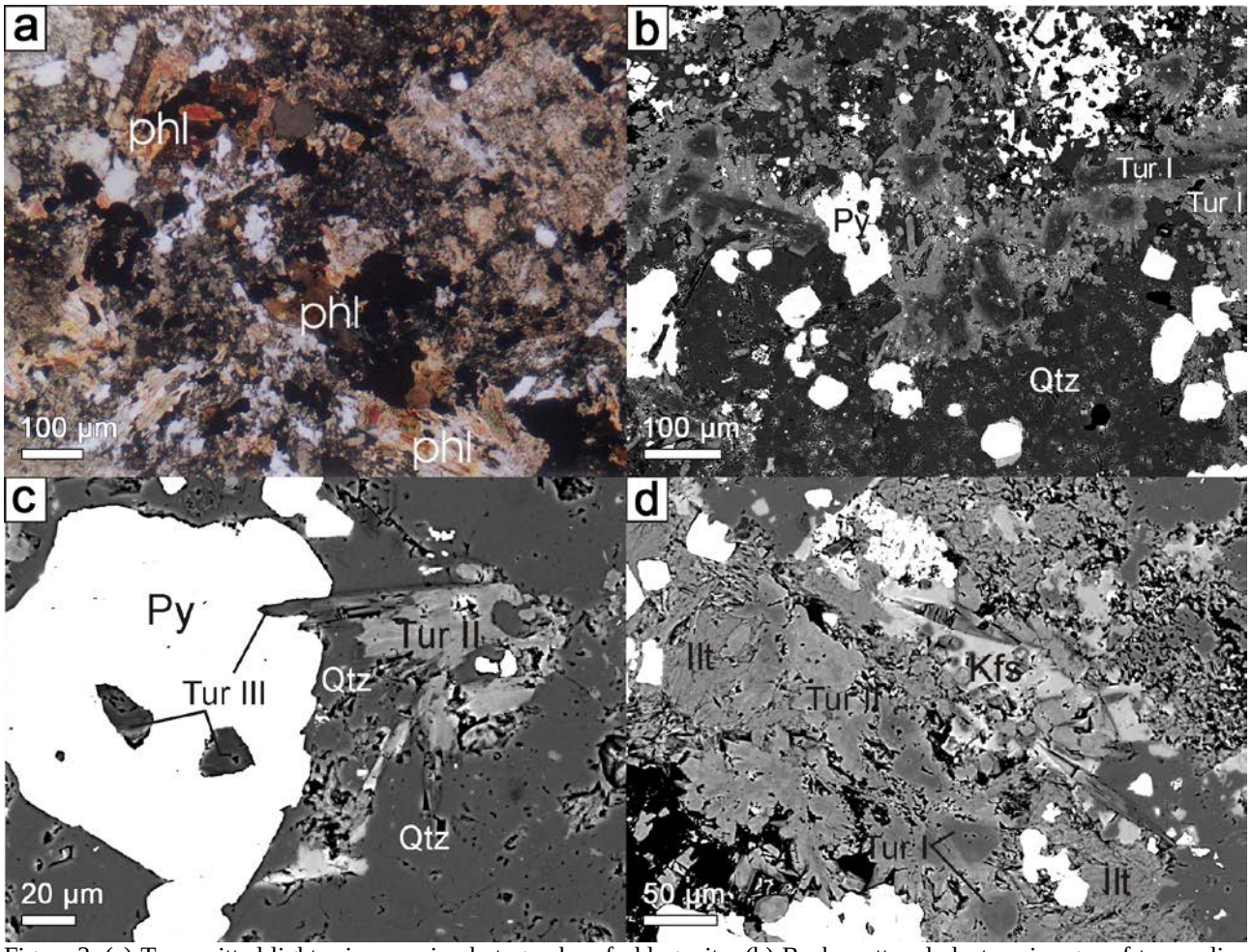

Figure 3. (a)-Transmitted light microscopic photography of phlogopite; (b)-Back-scattered electron images of tourmaline and illite, relatively large crystals of tourmaline I overgrown by tourmaline II; (c) - tourmaline III overgrows tourmaline II and embedded in pyrite; (d) - tourmaline II replaces earlier potassium feldspar, while illite fills interstices between crystals of tourmaline. Phl=phlogopite, Ilt = illite, Kfs = potassium feldspar, Py = pyrite, Qtz = quartz, Tur = tourmaline.

Table 1. Electron microprobe data for phlogopite from potassic alteration of Nistru deposit

Component	1	2	3	4	5	6	7	8	9	10	11	12
SiO_2	39.86	39.08	40.86	40.32	39.02	40.34	40.51	41.26	40.16	39.65	41.3	41.18
TiO_2	3.41	3.98	3.89	3.90	4.13	3.90	2.53	3.22	2.62	3.83	3.59	3.26
V_2O_3	0.04	b.d.l.	b.d.l.	b.d.l.	0.05	0.03	b.d.l.	b.d.l.	b.d.l.	0.11	0.03	0.07
Al_2O_3	11.94	12.69	12.12	12.45	12.21	12.58	11.66	12.00	12.55	12.64	12.11	11.93
FeO	9.55	9.21	7.76	8.85	8.87	6.08	8.9	7.16	9.35	8.78	5.50	7.72
MnO	0.05	0.04	0.08	b.d.l.	b.d.l.	0.12	0.06	0.04	b.d.l.	0.07	0.03	0.16
MgO	20.73	20.61	20.59	20.28	20.21	22.98	20.65	21.44	20.31	20.79	22.98	22.09
CaO	0.03	0.02	0.07	0.02	b.d.l.	b.d.l.	b.d.l.	0.06	0.03	0.01	0.02	0.07
K_2O	9.31	9.58	9.81	9.67	9.66	9.67	9.57	9.80	9.60	9.94	9.93	9.81
Na_2O	0.26	0.23	0.16	0.21	0.24	0.21	0.17	0.16	0.21	0.17	0.18	0.22
F	1.77	1.77	1.61	1.47	1.51	1.57	2.34	2.38	2.71	1.74	1.63	2.22
H_2O	3.28	3.29	3.40	3.46	3.37	3.47	2.98	3.04	2.83	3.33	3.45	3.14
2F = O	-0.75	-0.75	-0.68	-0.62	-0.64	-0.66	-0.98	-1.00	-1.14	-0.73	-0.69	-0.93
Total	99.48	99.75	99.67	100.01	98.63	100.29	98.38	99.56	99.23	100.33	100.06	100.94
Formulae calculated on the basis of 22 anions												
Si	2.900	2.839	2.942	2.907	2.864	2.869	2.971	2.965	2.927	2.861	2.933	2.931
^{IV}Al	1.024	1.087	1.028	1.058	1.056	1.055	1.008	1.016	1.078	1.075	1.014	1.001
Mg	2.249	2.232	2.210	2.180	2.212	2.437	2.258	2.297	2.207	2.236	2.433	2.344
Fe^{2+}_{tot}	0.581	0.560	0.468	0.534	0.545	0.362	0.546	0.431	0.570	0.530	0.327	0.460
Ti	0.187	0.217	0.211	0.211	0.228	0.209	0.139	0.174	0.144	0.201	0.192	0.174
V	0.002				0.003	0.002				0.006	0.002	0.004
Mn	0.003	0.002	0.005			0.007	0.004	0.002		0.004	0.002	0.010
K	0.864	0.888	0.901	0.889	0.905	0.877	0.895	0.898	0.893	0.915	0.900	0.891
Na	0.037	0.032	0.022	0.029	0.034	0.029	0.024	0.022	0.030	0.024	0.025	0.030
Ca	0.002	0.002	0.005	0.001	0	0	0	0.005	0.002	0.001	0.002	0.005
F	0.407	0.407	0.367	0.335	0.351	0.353	0.543	0.541	0.625	0.397	0.367	0.500
OH	1.593	1.593	1.633	1.665	1.649	1.647	1.457	1.459	1.375	1.603	1.634	1.500
$Fe_{tot}/(Fe_{tot}+Mg)$	0.21	0.20	0.17	0.20	0.20	0.13	0.19	0.16	0.21	0.19	0.12	0.16

Note: b.d.l. denotes that the content of the element is below detection limits, H_2O calculated by stoichiometry.

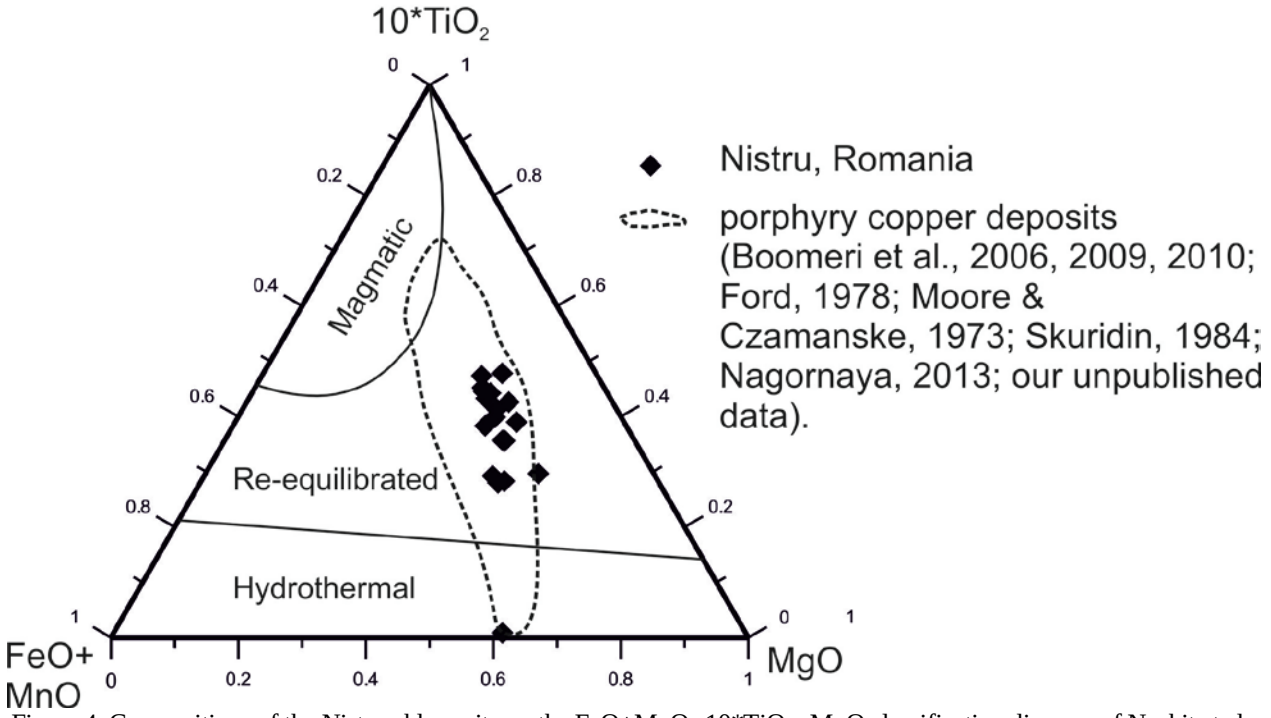

Figure 4. Compositions of the Nistru phlogopite on the FeO+MnO--10*TiO_2--MgO classification diagram of Nachit et al., 2005.

Tourmaline has been sampled from propylitic and phyllic alteration of porphyry quartz micro-monzodiorite. Tourmalines from the both alterations occur as fine acicular crystals and crystal aggregates enclosed in quartz. The length of individual crystal may exceed 100 μm (Fig. 3b). The crystals are pleochroic from green to dark green.

Electron microscopic observation revealed three generations of tourmaline (Figs. 3b to 3d) from propylitic alteration. Tourmaline I is the core of crystals; tourmaline II forms overgrowth rims and individual grains; and tourmaline III overgrows crystals of tourmaline II. Tourmaline II replaces potassium feldspar, whereas interstices between its crystals are filled by later illite (Fig. 3d). These two facts indicate that tourmaline II precipitated after potassium feldspar, but before illite. We did not observed relationship between potassium feldspar and tourmaline I, but tourmaline I could be assumed to crystallize close in time to potassium feldspar, because on the one hand tourmaline II overgrows tourmaline I and on the other hand, it replaces potassium feldspar.

Tourmalines I and II crystallized prior pyrite, whereas tourmaline III precipitated simultaneously with the latter. The chemical compositions of tourmalines studied are variable. The Fe content increases from the first (0.39-0.58 apfu) to the second generation (1.32-1.94 apfu) and decreases in the third generation (0.29-0.47 apfu) (Tables 2-4). At the same time, the Al content decreases from tourmaline I (6.49-6.93 apfu) to tourmaline II (5.56-5.98 apfu) and increases in the third generation (6.55-6.68 apfu). The similar behavior demonstrates the proportion of X-site vacancy. The Ca content increases from tourmaline I (0.03-0.15 apfu; only in two of eleven compositions this value exceeds 0.2 apfu) to tourmaline II (0.16-0.35) and decreases to tourmaline III (0.06-0.13 apfu).

On the ternary classification plot X-site vacancy--Ca—Na(+K) (Henry et al., 2011), all tourmaline compositions except for one fall into the alkali field (Fig. 5a). According to (Henry et al., 2011), this and calculated formulae allow classification of tourmaline I as dravite or oxy-dravite, one composition is referred to magnesio-foitite; tourmaline II is represented by schorl or dravite enriched in Ca, and tourmaline III is regarded as dravite. However, determination of Fe^{3+} in the tourmalines studied here could change this classification.

Tourmaline from phyllic alteration is similar in composition to tourmaline II from propylitic alteration. The Fe content in this tourmaline ranges from 1.57 to 1.91 apfu. The Al (5.85-6.03 apfu) and Ca (0.29-0.44 apfu) concentrations is also close to those in tourmaline II (Table 5). On the ternary classification plot X-site vacancy--Ca--Na(+K) (Henry et al., 2011), all compositions of this tourmaline plot in the alkali field. This and calculated formulae allow attribution of tourmaline to schorl enriched in Ca. However, determination of Fe^{3+} in the tourmaline studied could change this classification.

Table 2. Electron microprobe data for propylitic tourmaline I from Nistru deposit

Component	1	2	3	4	5	6	7	8	9	10	11
B_2O_3	10.83	10.95	10.87	10.63	10.86	10.98	10.93	11.18	11.02	10.94	10.93
SiO_2	36.35	37.00	36.89	36.53	37.52	38.12	37.01	38.56	38.11	37.31	36.84
TiO_2	0.34	b.d.l.	0.24	0.33	0.35	0.12	0.42	0.05	0.12	0.55	0.27
V_2O_3	0.37	0.32	0.35	0.70	1.09	b.d.l.	0.64	b.d.l.	0.13	0.45	0.40
Al_2O_3	35.47	37.05	36.27	33.10	34.52	35.34	36.08	35.47	35.45	34.64	36.52
FeO	3.65	3.39	3.69	4.29	3.50	2.94	3.34	1.23	0.63	3.83	3.71
MnO	b.d.l.	b.d.l.	b.d.l.	b.d.l.	b.d.l.	0.16	b.d.l.	b.d.l.	b.d.l.	0.07	0.05
MgO	7.92	7.21	7.17	7.99	7.71	8.28	7.49	10.10	9.71	8.2	7.22
CaO	1.26	1.00	0.85	0.81	0.48	0.54	0.88	0.16	0.18	1.44	0.83
Na_2O	1.57	1.42	1.53	1.29	1.52	1.73	1.29	2.14	1.92	1.29	1.45
F	b.d.l.	b.d.l.	0.09	0.05	b.d.l.	b.d.l.	b.d.l.	b.d.l.	b.d.l.	b.d.l.	b.d.l.
H_2O	3.33	3.31	3.25	3.40	3.40	3.45	3.38	3.66	3.51	3.39	3.39
2F = O	0	0	-0.04	-0.02	0	0	0	0	0	0	0
Total	101.09	101.65	101.16	99.10	100.95	101.66	101.46	102.55	100.78	102.11	101.61
Formulae calculated on the basis of 15 cations											
B	3.000	3.000	3.000	3.000	3.000	3.000	3.000	3.000	3.000	3.000	3.000
Si	5.835	5.873	5.894	5.967	6.002	6.031	5.885	5.994	6.011	5.928	5.859
^{T}Al	0.165	0.127	0.106	0.033	0	0	0.115	0.006	0	0.072	0.141
Total	6.000	6.000	6.000	6.000	6.002	6.031	6.000	6.000	6.011	6.000	6.000
^{Z}Al	6.000	6.000	6.000	6.000	6.000	6.000	6.000	6.000	6.000	6.000	6.000
Total Z	6.000	6.000	6.000	6.000	6.000	6.000	6.000	6.000	6.000	6.000	6.000
Mg	1.896	1.706	1.709	1.946	1.839	1.953	1.776	2.341	2.284	1.943	1.712
^{Y}Al	0.546	0.803	0.724	0.340	0.509	0.590	0.648	0.493	0.591	0.416	0.704
Fe^{2+}_{tot}	0.470	0.450	0.494	0.582	0.469	0.389	0.444	0.160	0.083	0.509	0.494
Ti	0.040	0	0.028	0.041	0.042	0.014	0.050	0.006	0.014	0.066	0.032
V	0.047	0.041	0.045	0.092	0.140	0.000	0.082	0.000	0.016	0.057	0.051
Mn	0	0	0	0	0	0.021	0	0	0	0.009	0.007
Total Y	2.999	3.000	3.000	3.001	2.999	2.967	3.000	3.000	2.988	3.000	3.000
Na	0.489	0.437	0.473	0.505	0.471	0.531	0.398	0.645	0.587	0.397	0.447
X-vacancy	0.294	0.392	0.382	0.354	0.447	0.377	0.452	0.328	0.383	0.357	0.411
Ca	0.217	0.171	0.145	0.141	0.082	0.092	0.150	0.027	0.030	0.246	0.142
Total X	1.000	1.000	1.000	1.000	1.000	1.000	1.000	1.000	1.000	1.000	1.000
$^{V}OH^-$	3.000	3.000	3.000	3.000	3.000	3.000	3.000	3.000	3.000	3.000	3.000
$^{W}OH^-$	0.567	0.503	0.472	0.708	0.627	0.647	0.587	0.803	0.693	0.598	0.605
$^{W}O^{2-}$	0.433	0.497	0.483	0.267	0.373	0.353	0.413	0.197	0.307	0.402	0.395
F	0	0	-0.045	-0.025	0	0	0	0	0	0	0
Total W	1.000	1.000	1.000	1.000	1.000	1.000	1.000	1.000	1.000	1.000	1.000
Al_{tot}	6.711	6.931	6.830	6.373	6.509	6.590	6.763	6.499	6.591	6.487	6.846
$Fe_{tot}/(Fe_{tot}+Mg)$	0.12	0.13	0.14	0.15	0.20	0.17	0.20	0.06	0.04	0.21	0.22
Ca/(Ca+Na)	0.31	0.28	0.23	0.22	0.15	0.15	0.27	0.04	0.05	0.38	0.24
X-vac/(X-vac+Na)	0.38	0.47	0.45	0.41	0.49	0.42	0.53	0.34	0.39	0.47	0.48

Note: In Tables 2-4 b.d.l. denotes that the content of the element is below detection limits, H_2O and B_2O_3 calculated by stoichiometry, Fe^{2+} and Fe^{3+} calculated from charge balance constraints.

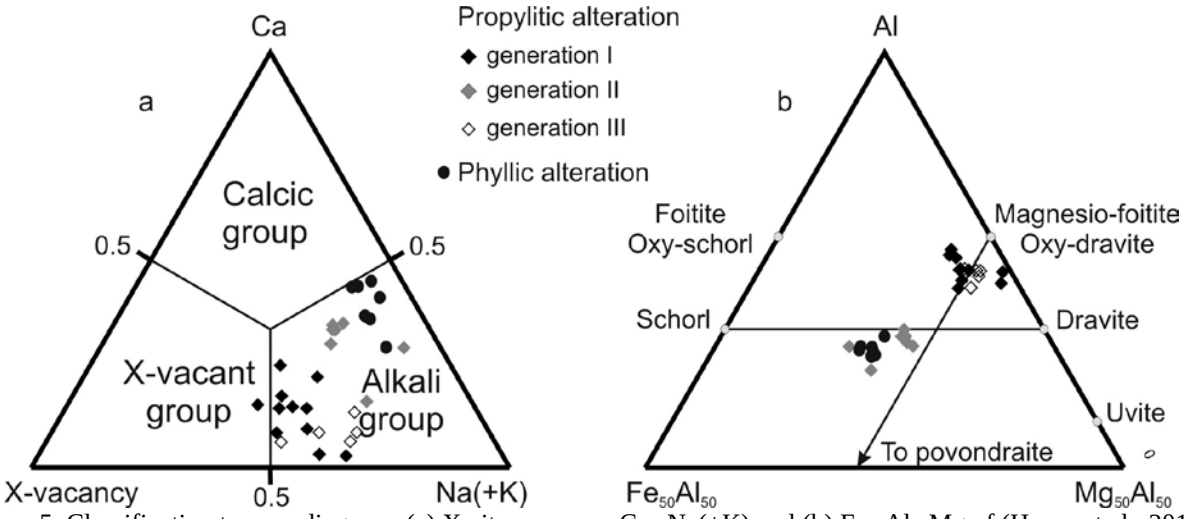

Figure 5. Classification ternary diagrams (a) X-site vacancy--Ca--Na(+K) and (b) Fe--Al--Mg of (Henry et al., 2011), for tourmalines from the Nistru deposit.

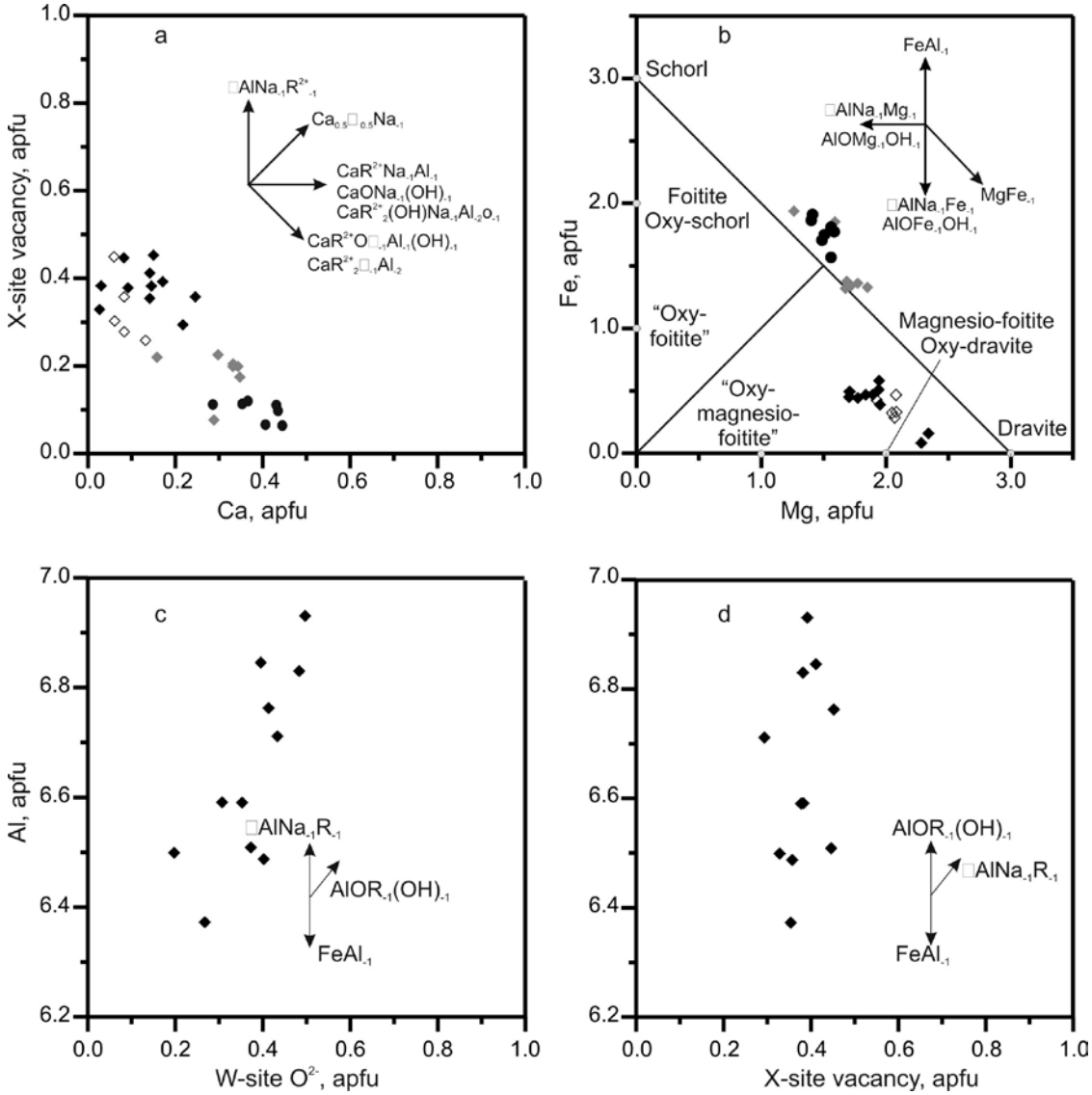

Figure 6. Various binary diagrams showing data for tourmaline from the Nistru deposit. (a) Ca *versus* X-site vacancy diagram.; (b) Mg *versus* Fe diagram; (c) W-site O^{2-} *versus* Al diagram for tourmaline I; (d) *X*-site vacancy *versus* Al diagram for tourmaline I. The directions of selected exchange-vectors are given for reference. The locations of end-member "oxy-foitite", foitite, oxy-schorl, and schorl are shown by the grey circles. See Figure 5 for legend.

Table 3. Electron microprobe data for propylitic tourmaline II from Nistru deposit

Component	1	2	3	4	5	6	7
B_2O_3	10.47	10.11	10.15	10.50	10.27	10.38	10.32
SiO_2	35.61	34.62	34.50	35.77	35.09	35.30	35.04
TiO_2	0.68	0.00	0.37	0.69	0.54	0.58	0.68
V_2O_3	0.00	0.00	0.29	0.23	0.23	0.24	0.23
Al_2O_3	29.74	28.84	27.52	30.25	29.58	29.62	30.14
FeO	9.56	13.47	12.92	9.94	9.46	9.71	9.36
MgO	7.48	4.94	6.23	6.84	6.82	7.11	6.68
CaO	1.95	0.86	1.57	1.87	1.83	1.91	1.65
Na_2O	1.49	1.87	1.91	1.47	1.41	1.41	1.46
F	b.d.l.	b.d.l.	b.d.l.	0.15	0.18	0.29	0.27
H_2O	3.61	3.48	3.50	3.48	3.39	3.44	3.37
2F = O	0	0	0	-0.06	-0.08	-0.12	-0.11
Total	100.57	98.18	98.97	101.13	98.71	99.87	99.09
Formulae calculated on the basis of 15 cations							
B	3.000	3.000	3.000	3.000	3.000	3.000	3.000
Si	5.913	5.952	5.910	5.919	5.939	5.911	5.901
^{T}Al	0.087	0.048	0.090	0.081	0.061	0.089	0.099
Total	6.000	6.000	6.000	6.000	6.000	6.000	6.000
^{Z}Al	5.734	5.796	5.467	5.819	5.839	5.757	5.885
^{Z}Mg	0.266	0.204	0.533	0.181	0.161	0.243	0.115
Total Z	6.000	6.000	6.000	6.000	6.000	6.000	6.000
^{Y}Mg	1.587	1.061	1.059	1.507	1.560	1.532	1.562
Fe^{2+}	1.318	1.626	1.578	1.377	1.341	1.353	1.320
Fe^{3+}	0.010	0.313	0.275	0	0	0.008	0
Ti	0.084	0	0.048	0.086	0.069	0.074	0.087
V	0	0	0.040	0.030	0.031	0.033	0.032
Total Y	2.999	3.000	2.999	3.000	3.000	3.001	3.001
Na	0.479	0.623	0.636	0.470	0.464	0.459	0.478
Ca	0.347	0.158	0.288	0.331	0.332	0.343	0.297
X-vacancy	0.174	0.219	0.076	0.199	0.204	0.198	0.225
Total X	1.000	1.000	1.000	1.000	1.000	1.000	1.000
$^{V}OH^{-}$	3.000	3.000	3.000	3.000	3.000	3.000	3.000
$^{W}OH^{-}$	1.000	1.000	1.000	0.849	0.829	0.845	0.793
$^{W}O^{2-}$	0	0	0	0.074	0.073	0	0.063
$^{W}F^{-}$	0	0	0	0.077	0.098	0.155	0.144
Total W	1.000	1.000	1.000	1.000	1.000	1.000	1.000
Al	5.821	5.844	5.557	5.900	5.900	5.846	5.983
Fe_{tot}	1.328	1.939	1.853	1.377	1.341	1.361	1.320
Mg	1.853	1.265	1.592	1.688	1.721	1.776	1.677
$Fe_{tot}/(Fe_{tot}+Mg)$	0.36	0.77	0.58	0.41	0.39	0.38	0.39
Ca/(Ca+Na)	0.42	0.20	0.31	0.41	0.42	0.43	0.38
X-vac/(X-vac+ Na)	0.27	0.26	0.11	0.30	0.31	0.30	0.32

For notes see Table 2

Isomorphic substitutions in tourmalines. The compositions of the examined propylitic tourmaline generations and phyllic tourmaline are parallel to the $CaR^{2+}O\square_{-1}Al_{-1}(OH)_{-1}$ and $CaR_2\square_{-1}Al_{-2}$ (R = Fe_{tot}, Mg) exchange vectors in the binary X-site vacancy versus Ca (Fig. 6a). These vectors correspond to the chemical substitutions of $^{X}Ca + {}^{Y}R^{2+} + {}^{W}O^{2-} \rightarrow {}^{X}\square + {}^{Y}Al + {}^{W}OH^{-}$ and $^{X}Ca + {}^{Y}R^{2+} + {}^{Z}R^{2+} \rightarrow {}^{X}\square + {}^{Y}Al + {}^{Z}Al$, respectively.

On the ternary plot Fe-Al-Mg (Fig. 5b), the compositions of tourmaline I and III are above the schorl-dravite join, whereas those of tourmaline II and phyllic tourmaline are below this join. In the first case, this position indirectly indicates low Fe^{3+} in the tourmalines, whereas in the second case, the position below the join indicates the enrichment of tourmaline II in Fe^{3+}.

On the diagram Fe versus Mg (Fig. 6b), the compositions of tourmaline I are parallel to the $AlOMg_{-1}(OH)_{-1}$ and $Al^{X}\square Mg_{-1}Na_{-1}$. We have used binary Al versus O and Al versus X-site vacancy

diagram to estimate which vector is predominant (Figs. 6c, 6d). These data demonstrate that the positive correlation between Al and O^{2-} (correlation coefficient = 0.73) is stronger than that between Al and X-site vacancy (correlation coefficient = 0.37), which means that the substitution $Al + O^{2-} \rightarrow Mg + OH^-$ is more preferable. In addition, the content of Fe and Mg are negatively correlated (correlation coefficient = -0.78). This corresponds to the $Fe \rightarrow Mg$ chemical substitution. Thus, tourmaline I is characterized by the combination of two types of isomorphic substitutions $Al + O^{2-} \rightarrow Mg + OH^-$ and $Fe \rightarrow Mg$.

The compositions of tourmaline II and phyllic tourmalines are nearly parallel to the schorl--dravite join (Fig. 6b) reflecting effect of the exchange vector $FeMg_{-1}$ corresponding to the chemical substitution Fe^{2+} for Mg^{2+}. Correlation coefficient between Fe_{tot} and Mg is -0.85 and -0.62, respectively.

Due to few measured compositions of tourmaline III we cannot reliably determine the chemical substitutions in it. However, there is insignificant positive correlation between Ca + Mg + Fe and 2Al + X-site vacancy (correlation coefficient -0.81). This corresponds to the chemical substitution $Ca + Mg + Fe \rightarrow 2Al + X\text{-site}$.

Table 4. Electron microprobe data for propylitic tourmaline III from Nistru deposit

Component	1	2	3	4	5
B_2O_3	10.85	10.63	10.67	10.84	10.77
SiO_2	36.97	36.30	36.70	37.53	36.74
TiO_2	0.17	0.36	0.35	0.11	0.23
V_2O_3	0.14	0.18	0.15	0.09	0.16
Al_2O_3	35.35	33.51	34.40	34.68	35.14
FeO	2.42	3.42	2.10	2.47	3.15
MgO	8.59	8.55	8.53	8.72	8.02
CaO	0.35	0.75	0.48	0.36	0.48
Na_2O	1.58	1.93	2.03	2.05	1.79
K_2O	0.00	0.00	0.16	0.10	0.00
F	0.03	b.d.l.	b.d.l.	b.d.l.	b.d.l.
H_2O	3.62	3.52	3.42	3.43	3.49
2F = O	-0.01	0	0	0	0
Total	100.06	99.15	98.99	100.38	99.97
Formulae calculated on the basis of 15 cations					
B	3.000	3.000	3.000	3.000	3.000
Si	5.918	5.930	5.977	6.012	5.923
^{T}Al	0.082	0.070	0.023	0	0.077
Total T	6.000	6.000	6.000	6.000	6.000
^{Z}Al	6.000	6.000	6.000	6.000	6.000
^{Y}Al	0.587	0.382	0.579	0.548	0.599
Mg	2.051	2.082	2.071	2.084	1.928
Fe^{2+}	0.324	0.468	0.286	0.333	0.425
V	0.018	0.024	0.020	0.011	0.020
Ti	0.021	0.044	0.043	0.013	0.027
Total Y	3.001	3.000	2.999	2.989	2.999
Na	0.492	0.610	0.639	0.637	0.560
X-vacancy	0.448	0.258	0.244	0.282	0.357
Ca	0.060	0.132	0.083	0.061	0.083
K	0	0	0.034	0.020	0
Total X	1.000	1.000	1.000	1.000	1.000
^{V}OH	3.000	3.000	3.000	3.000	3.000
^{W}OH	0.809	0.702	0.532	0.630	0.677
O^{2-}	0.176	0.298	0.468	0.370	0.323
F	0.015	0	0	0	0
Total W	1.000	1.000	1.000	1.000	1.000
Al_{tot}	6.669	6.452	6.602	6.548	6.776
$Fe_{tot}/(Fe_{tot}+Mg)$	0.14	0.18	0.12	0.14	0.18
Ca/(Ca+Na)	0.11	0.18	0.11	0.09	0.13
X-vac/(X-vac+Na)	0.48	0.30	0.28	0.31	0.39

See Table 2 for notes

Table 5. Electron microprobe data for tourmaline from phyllic alteration at Nistru deposit

Component	1	2	3	4	5	6	7
B_2O_3	10.23	10.21	10.32	10.20	10.18	10.23	10.20
SiO_2	33.77	33.61	34.26	35.79	33.32	33.89	33.54
TiO_2	0.05	0.04	0.35	0.05	0.04	0.09	0.17
Cr_2O_3	0.07	0.51	b.d.l.	b.d.l.	b.d.l.	b.d.l.	0.11
V_2O_3	0.00	0.13	0.12	0.04	0.03	0.00	0.06
Al_2O_3	29.76	29.50	30.39	28.29	29.62	29.18	29.21
MnO	0.11	0.07	0.07	0.07	0.08	0.07	0.09
FeO	13.12	12.28	11.14	11.97	13.38	12.73	12.44
MgO	5.54	5.94	6.22	5.86	5.55	6.16	6.25
CaO	2.00	2.38	1.58	2.35	1.92	2.23	2.43
K_2O	0.00	0.03	0.06	0.05	0.04	0.04	0.05
Na_2O	1.56	1.40	1.81	1.36	1.59	1.58	1.46
F	0.00	0.00	0.10	0.57	0.38	0.42	0.18
H_2O	3.53	3.52	3.56	3.07	3.33	3.33	3.43
2F = O	0	0	0.04	0.24	0.16	0.18	0.08
Total	99.76	99.63	99.89	99.19	99.13	99.60	99.47
Formulae calculated on the basis of 15 cations							
B	3.000	3.000	3.000	3.000	3.000	3.000	3.000
Si	5.738	5.720	5.768	6.099	5.691	5.760	5.714
^{T}Al	0.262	0.280	0.232	0	0.309	0.240	0.286
Total	6.000	6.000	6.000	6.000	6.000	6.000	6.000
^{Z}Al	5.698	5.639	5.799	5.682	5.653	5.606	5.580
^{Z}Mg	0.302	0.361	0.201	0.318	0.347	0.394	0.420
Total Z	6.000	6.000	6.000	6.000	6.000	6.000	6.000
^{Y}Mg	1.102	1.148	1.360	1.172	1.066	1.168	1.167
Fe^{2+}	1.540	1.525	1.395	1.707	1.489	1.521	1.492
Fe^{3+}	0.326	0.225	0.174	0	0.424	0.290	0.282
Ti	0.007	0.005	0.044	0.007	0.005	0.012	0.022
V	0.000	0.018	0.017	0.006	0.004	0	0.008
Cr	0.010	0.069	0	0	0	0	0.015
Mn	0.001	0.001	0.001	0.001	0.001	0.001	0.001
Total Y	2.986	2.991	2.991	2.893	2.989	2.992	2.987
Na	0.515	0.462	0.590	0.448	0.525	0.520	0.481
Ca	0.365	0.435	0.286	0.431	0.353	0.406	0.444
X-vacancy	0.120	0.096	0.111	0.110	0.113	0.065	0.064
K	0.000	0.007	0.013	0.011	0.009	0.009	0.011
Total X	1.000	1.000	1.000	1.000	1.000	1.000	1.000
$^{V}OH^-$	3.000	3.000	3.000	3.000	3.000	3.000	3.000
$^{W}OH^-$	1.000	1.000	1.000	0.492	0.795	0.773	0.901
$^{W}O^{2-}$	0	0	0	0.200	0	0	0
$^{W}F^-$	0	0	0.055	0.308	0.205	0.227	0.099
Total W	1.000	1.000	1.000	1.000	1.000	1.000	1.000
Al	5.961	5.919	6.031	5.682	5.962	5.846	5.866
Fe_{tot}	1.865	1.750	1.569	1.707	1.912	1.810	1.774
Mg	1.404	1.508	1.561	1.489	1.413	1.562	1.587
$Fe_{tot}/(Fe_{tot}+Mg)$	0.57	0.54	0.50	0.53	0.58	0.54	0.53
Ca/(Ca+Na)	0.41	0.48	0.33	0.49	0.40	0.44	0.48
X-vac/(X-vac+ Na)	0.19	0.17	0.16	0.20	0.18	0.11	0.12

For notes see Table 2

Illite occurring as aggregates of fine flakes reaching 50 μm in size (Fig. 3d) precipitated after tourmaline. The mineral contains insignificant F (0.06-0.08 apfu F); the $Fe_{tot}/(Fe_{tot}+Mg)$ ranges from 0.13 to 0.25. The representative electron microprobe data are given in table 6. The Si content in illite studied is higher than 3.25 apfu therefore the mineral is regarded as phengitic illite.

Table 6. Representative electron microprobe data for phyllic illite from Nistru deposit

Component	1	2	3	4	5
SiO_2	54.02	52.01	51.03	52.03	51.98
TiO_2	0.06	0.13	0.13	0.16	0.14
V_2O_3	0.17	0.08	0.11	0.12	0.05
Al_2O_3	29.56	32.85	32.11	32.31	32.75
FeO_{tot}	2.10	0.70	0.83	0.69	0.61
MgO	3.51	2.38	2.34	2.32	2.22
CaO	0.38	0.09	0.08	0.09	0.07
K_2O	7.61	9.77	9.84	9.66	9.58
Na_2O	0.13	0.17	0.19	0.16	0.18
F	0.31	0.30	0.26	0.40	0.38
H_2O	4.57	4.57	4.50	4.50	4.51
2F = O	0.13	0.17	0.13	0.11	0.17
Total	101.98	102.62	101.05	101.87	101.93
Formula calculated on the basis of 22 anions					
Si	3.431	3.306	3.303	3.326	3.318
^{IV}Al	0.569	0.694	0.697	0.674	0.682
Total	4.000	4.000	4.000	4.000	4.000
^{VI}Al	1.644	1.767	1.753	1.761	1.782
Mg	0.332	0.226	0.226	0.221	0.211
Fe	0.112	0.037	0.045	0.037	0.033
Ti	0.003	0.006	0.006	0.008	0.007
V	0.009	0.004	0.006	0.006	0.003
Total	2.100	2.040	2.036	2.033	2.036
K	0.617	0.792	0.813	0.788	0.780
Na	0.016	0.021	0.024	0.020	0.022
Ca	0.026	0.006	0.005	0.006	0.005
Total	0.659	0.819	0.842	0.814	0.807
OH	1.938	1.940	1.947	1.919	1.923
F	0.062	0.060	0.053	0.081	0.078
Total	2.000	2.000	2.000	2.000	2.000
Al_{tot}	2.213	2.461	2.450	2.435	2.464
$Fe_{tot}/(Fe_{tot}+Mg)$	0.25	0.14	0.17	0.14	0.13

Note: H_2O calculated by stoichiometry

5. DISCUSSION

This study demonstrates for the first time the presence of requilibrated biotite (phlogopite) at Nistru, with composition typical to that from potassic alteration zones of porphyry copper deposits elsewhere (Nachit et al., 2005; Boomeri et al., 2006, 2009, 2010; Ford, 1978; Moore et al., 1973; Skuridin, 1984; Nagornaya, 2013).

The relationships with potassium feldspar and illite indicate that tourmalines II and III from propylitic zone postdate the former and predate the latter. Tourmaline I could crystallize close in time to potassium feldspar.

Tourmaline I is characterized by the $Al + O^{2-} \rightarrow Mg + OH^-$ chemical substitution which is rare in tourmaline; this was found in tourmalines from plagioclase--muscovite--scapolite metaevaporite layers in dolomite marble near Prosetín, Czech Republic (Bačik et al., 2012). However, no metaevaporites were reported from the Nistru area. Tourmaline with $Al + O^{2-} \rightarrow Mg + OH^-$ has been also found at the flank of the Lora porphyry copper deposit, Chukchi Peninsula, Russia (our unpublished data). No associated ore minerals were identified with this tourmaline. Tourmaline grains are overgrown by rare second generation tourmaline whose composition corresponds to that of typical porphyry tourmaline (Baksheev et al., 2012c). Therefore we suggest that isomorphic substitution $Al + O^{2-} \rightarrow Mg + OH^-$ is probably typical of barren tourmalines.

Tourmaline II from propylite and tourmaline from phyllic alteration are similar in the composition and character of isomorphic substitution. Therefore, we consider that these tourmalines are simultaneous, crystallized at the propylitic stage and tourmaline from phyllic zone is relict in regard to phyllic alteration.

Ferric-rich tourmaline from propylitic alteration was described from porphyry copper and gold deposits (Baksheev et al., 2010, 2011), in the Berezovskoe gold (Kudryavtseva & Baksheev, 2003) and Shabry talc (Baksheev et al., 2012a) deposits in the Central Urals. The two last deposits are not porphyry. Propylitic tourmaline from porphyry copper deposits is characterized by the Al → Fe^{3+} isomorphic substitution, whereas that from the Berezovskoe and Shabry is distinguished by the Mg → Fe^{2+} with the minor role of the former substitution. Taking into account this data, we suggest that propylite at the Nistru deposit is not related to the porphyry system.

The enrichment in ferric iron of tourmaline II and relict tourmaline from phyllic alteration is explained by higher fO_2 during the formation of these tourmalines than that during the crystallization of tourmaline I and III. The higher fO_2 could be resulted from incursion of meteoric oxygenated fluids in the system or arising from boiling, causing the loss of H_2 into the vapor phase, resulting in the oxidation of Fe in the aqueous phase (Yang & Jang 2002). Then, during precipitation of the generation III tourmaline, the gradual increase in H_2S in the mineralizing fluid results in a reduction of Fe^{3+} to Fe^{2+}, and then, the latter is partitioned into sulfides rather than in tourmaline. The precipitation of sulfides leads to a decrease in $Fe_{tot}/(Fe_{tot} + Mg)$ value in tourmaline of generation III, in comparison with tourmaline II.

Taking into account the aforementioned evidences, we consider that tourmalines I and II at the Nistru deposit are early and not accompanied by any ore mineralization, whereas tourmaline III precipitated at the end of propylitic stage accompanied with crystallization of pyrite. Negligible ore constituents (pyrite, fahlores, bornite) accompanying not porphyry propylite are described from the Shabry talc deposit in the Urals (Filimonov, 2009).

Illite is a rock-forming mineral of phyllic to intermediate argillic alteration. In the Si *versus* Al diagram (Fig. 7), the compositions of the mineral studied here plot on the region of overlap of argillic illite related to porphyry system and epithermal volcanogenic Au-Ag deposits.

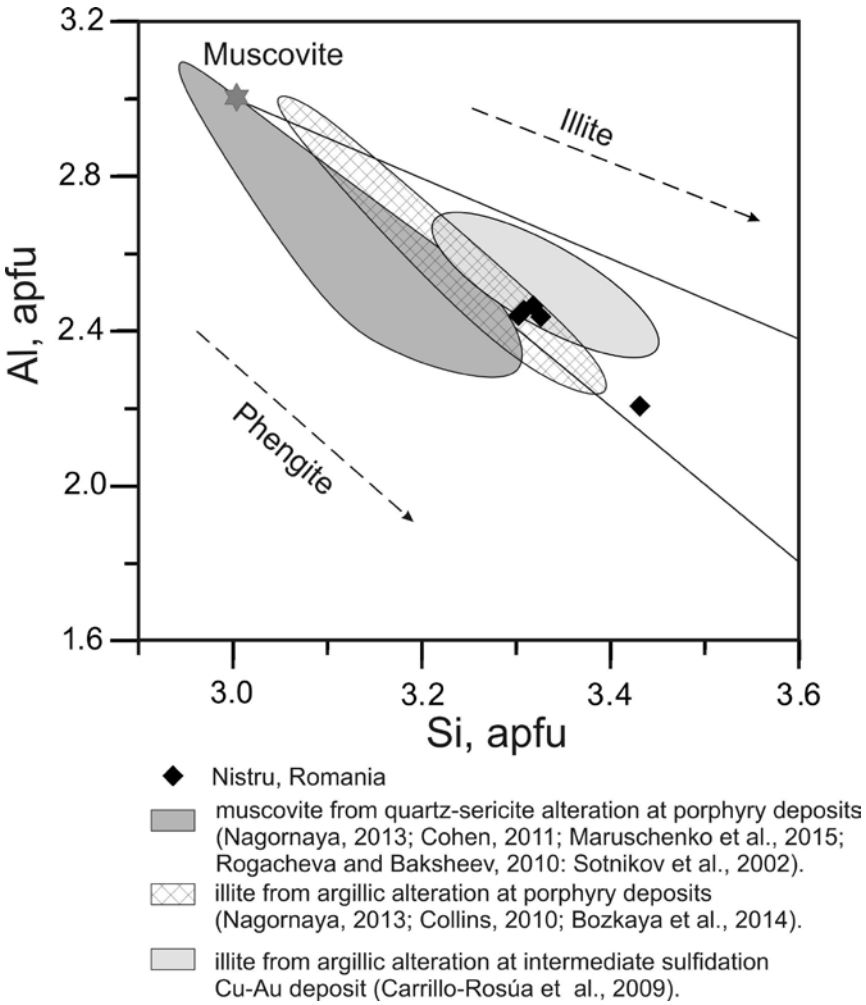

Figure 7. A Si *versus* Al diagram for illite from the Nistru deposit.

Summarizing all aforementioned evidences, we suggest that the Nistru deposit is complex with the early porphyry stage related to porphyry quartz micro-monzodiorite stock. The later tourmaline-bearing propylite postdating the intrusion of porphyry quartz microdiorite could be accompanied by negligible ore mineralization. The formation of illite is caused by the latest epithermal volcanogenic fluid responsible for the base metal and Au-Ag mineralization. This fluid is probably related to subvolcanic quartz andesite, (Fig. 1B).

6. CONCLUSIONS

In the Nistru zone, southern part of the Gutîi Mountains three hydrothermal stages was identified: (1) early porphyry related to

porphyry quartz micro-monzodiorite and not mentioned so far, (2) later propylitic related to porphyry quartz microdiorite and accompanying minor ore mineralization, and (3) epithermal volcanogenic accompanying the base and precious metal mineralization.

The minerals studied here belong to three different alterations: potassic, phyllic and intermediate argillic. The chemical composition of biotite supports the porphyry stage at the Nistru deposit. The composition of tourmaline and character of chemical substitution in this mineral suggest the presence of early tourmaline beyond association with any ore minerals (barren tourmaline) and later propylitic tourmaline associated minor sulfides.

Acknowledgments

We thank Panagiotis Voudouris for his constructive comments, which have significantly improved the paper.

REFERENCES

Bačik, Peter, Uher, Pavel, Cempírek, Jan, & Vaculovič, Tomáš, 2012. *Magnesian tourmalines from plagioclase-muscovite-scapolite metaevaporite layers in dolomite marbles near Prosetín (Olešnice Unit, Moravicum, Czech Republic,* Journal of Geosciences, Vol. 57, No. 3, 143-153.

Baksheev, I.A., Chitalin, A.F., Yapaskurt, V.O., Vigasina, M.F., Bryzgalov, I.A., Ustinov, V.I., 2010. *Tourmaline in the Vetka porphyry copper–molybdenum deposit of the Chukchi Peninsula of Russia.* Moscow Univ. Geol. Bull., 65, 27–38.

Baksheev, I.A., Erokhin, Yu.V., Vigasina, M.F., & Bryzgalov, I.A., 2012a. *Tourmaline from propylite of the Shabry deposit, Central Urals.* Zap. Ross. Mineral. O-va. No. 3, 68–83 (in Russian).

Baksheev, I. A., Plotinskaya, O. Yu., Yapaskurt, V. O., Vigasina, M. F., Bryzgalov, I. A., Groznova, E. O., & Marushchenko, L. I. 2012b. *Tourmaline from Deposits of the Birgil'da–Tomino Ore Cluster, South Urals,* Geology of Ore Deposits, 54, 458-473.

Baksheev, I. A. Prokof'ev, V.Yu., Zaraisky, G.P., Chitalin, A.F., Yapaskurt, V.O., Nikolaev, Y.N., Tikhomirov, P.L., Nagornaya, E.V., Rogacheva, L.I., Gorelikova, N.V., & Kononov, O.V., 2012c. *Tourmaline as a prospecting guide for the porphyry-style deposits.* European Journal of Mineralogy, Vol. 24, No. 6, 957-979.

Baksheev, I. A., Prokof'ev, V.Yu., Yapaskurt ,V. O., Vigasina, M. F., Zorina, L. D., Solov'ev, V. N., 2011. *Ferric-iron-rich tourmaline from the Darasun gold deposit, Transbaikalia, Russia,* Canadian Mineralogist, Vol. 49, 263–276.

Boomeri, M., Mizuta, T., Ishiyama, D., & Nakashima, K., 2006. *Fluorine and chlorine in biotite from the Sarnwosar granitic rocks, Northeastern Iran.* Iranian Journal of Science & Technology, Transaction A, 30 (A1), 111-125.

Boomeri, M., Nakashima, K., & Lentz, D.R., 2010. *The Sarcheshmeh porphyry copper deposit, Kerman, Iran: A mineralogical analysis of the igneous rocks and alteration zones including halogen element systematic related to Cu mineralization processes.* Ore Geology Reviews, Vol. 38, No. 4, 367–381.

Boomeri, M., Nakashima, K., & Lentz, D.R., 2009. *The Miduk porphyry Cu deposit, Kerman, Iran: A geochemical analysis of the potassic zone including halogen element systematics related to Cu mineralization processes.* Journal of Geochemical Exploration, 103, (1), 17–29.

Borcoş, M., Gheorhiţă, I., Lang, B., 1974. *Neogene hydrothermal ore deposits in the volcanic Gutîi Mountains I. Ilba-Băiţa Metallogenic District,* Revue Roumaine de Géologie Géophysique et Géographie, Série de Géologie, 18, 19-37.

Borcoş, M., Lang, B., Peltz, S., Stan, N., 1972a. *The evolution of the Neogen volcanism in the western part of Gutâi Mts. (Negreşti - Seini - Băiţa).* Studii tehnice şi economice, Seria I, Mineralogie-Petrografie, No. 6, 7-35, Institutul Geologic Bucureşti, (in Romanian with French summary).

Borcoş, M., Gheorghiţă, I., Lang, B., Stan, N., Volanschi, E., Mîndroiu, V., 1972b. *Considerations regarding the association of the metallogenetic activity with Sarmatian pyroxene andesites from SW of Gutii Mountains (Ilba-Nistru-Băiţa).* Studii Tehnice şi Economice, Seria I, No. 6, 65-88, Mineralogie-Petrografie, Institutul Geologic Bucureşti, (in Romanian with English summary).

Bozkaya, G., HanilçI, N., Baksheev, I. A., Prokofiev, V. Yu. and Banks, D. A. 2014. *Tourmaline composition of the Kýþladağ Au Deposit, Uþak, Turkey.* Acta Geologica Sinica, (English Edition),Vol. 88, (supp. 2), 520–521.

Carrillo-Rosúa, J., Morales-Ruano, S., Esteban-Arispe, I. & Hach-Alí, P.F., 2009. *Significance of phyllosilicate mineralogy and mineral chemistry in the epithermal environment. Insights from the Palai-Islica Au-Cu deposit (Almería, SE Spain).* Clays and Clay Minerals, Vol. 57, No.1, 1–24.

Cohen, J.F., 2011. *Mineralogy and geochemistry of hydrothermal alteration at the Ann-Mason porphyry copper deposit, Nevada: Comparison of large scale ore exploration techniques to mineral chemistry*, MS thesis, Oregan State University.

Collins, A. C., 2010. *Mineralogy and geochemistry of tourmaline in contrasting hydrothermal systems: Copiapó Area, Northern Chile,* MS thesis, University of Arizona, pages 225.

Damian, F., 1999. *Bismuth minerals-native gold association in the copper mineralisation from Nistru-Baia Mare zone.* Studia Universitatis Babeş-Bolyai, Cluj-Napoca, Geologia, XLIV, 1, 151-158.

Damian, F., 2000. *The evolution of the magmatic and*

metallogenetic processes in the Nistru area (Gutîi Mountains). Mineralia Slovaca, 32, 236-264.

Damian, F., 2003. *The mineralogical characteristics and the zoning of the hydrothermal types alteration from Nistru ore deposit, Baia Mare Metallogenetic district.* Studia Universitatis Babeş-Bolyai, Geologia, XLVIII, 1, 101–112.

Damian, F., Damian, Gh., Constantina, C., 2009. *The subvolcanic magmatic rocks from the Nistru zone (Gutîi Mountains).* Carpathian Journal of Earth and Environmental Sciences, Vol. 4, No. 2, 101-122.

Dutrow, Barbara L., & Henry, Darrell J., 2000. *Complexly zoned fibrous tourmaline, Cruzeiro mine, Minas Gerais, Brazil: a record of evolving magmatic and hydrothermal fluids.* The Canadian Mineralogist, Vol. 38, No.1, 131-143.

Edelstein, O., Bernad, A., Kovacs, M., Crihan, M., Pécskay, Z., 1992. *Preliminary date regarding the K-Ar ages of some eruptive rocks from Baia Mare Neogene volcanic zone.* Revue Roumaine de Géologie, 36, 45-60.

Filimonov, S.V. 2009. *The fahlore-group minerals as guides of mineralizing process: a case study of hydrothermal gold deposits*. Unpub. PhD thesis. MSU, Moscow. 183 p. (in Russian).

Ford, J. H., 1978. *A chemical study of alteration at the Panguna porphyry copper deposit, Bougainville Papua New Guinea.* Economic Geology, Vol. 73, No. 5, 703-720.

Harangi, Szabolcs, Downes, Hilary & Seghedi, I. 2006.Tertiary- Quaternary subduction processes and related magmatism in the Alpine-Mediterranean region. In: Gee, D.G. and Stephenson, R. (eds.) European lithosphere dynamics. Geological Society of London Memoir 32. London: Geological Society of London, p. 167-190. ISBN 978- 1-86239-212-0.

Henry, D.J., Novák, M., Hawthorne, F.C., Ertl, A., Dutrow, B.L., Uher, P. & Pezzotta, F., 2011. *Nomenclature of the tourmaline-supergroup minerals.* American Mineralogist, 96, 895-913.

Kudryavtseva, O.E. & Baksheev, I.A. 2003. *Compositional variations in tourmaline from the Berezovskoe gold deposit, Central Urals.* Zap. Ross. Mineral. O-va, No. 3, 108–125 (in Russian).

Lynch, G. & Ortega, S. 1997. *Hydrothermal alteration and tourmaline-albite equilibrium at the Coxheath porphyry Cu-Mo-Au deposit, Nova Scotia*, Canadian Mineralogist, 35, 79–94.

Marcoux, E., Grancea, L., Lupulescu, M. & Milési, J.P., 2002. *Lead isotope signatures of epithermal and porphyry-type ore deposits from the Romanian Carpathian Mountains.* Mineralium Deposita, 37, 173–184.

Maruschenko, L.I., Baksheev, I. A., Nagornaya, E.V., Chitalin, A. F., Nikolaev, Yu. N., Kal`ko, I.A., & Prokofiev, V.Yu., 2015. *Quartz-sericite and argillic alterations at the Peschanka Cu-Mo-Au deposit, Chukchi Peninsula, Rusia,* Geology of Ore Deposits, Vol. 57, No. 3, 213-225.

Mason, Paul R.D., Seghedi, Ioan, Szákacs, Alexandru, Downes, Hilary 1998. Magmatic constraints on geodynamic models of subduction in the East Carpathians, Romania, Tectonophysics 297, 157–176.

Meyer, Charles & Hemley, Julian J., 1967. *Wall rock alteration*. in Barnes Hubert Lloyd edited, Geochemistry of Hydrothermal Ore Deposits, pp. 166-235, Holt, Rinehart and Winston Inc. New York, Chicago, San Francisco, Atlanta, Dallas, Montreal, Toronto, London.

Moore, W. J. & Czamanske, G.K., 1973. *Compositions of biotites from unaltered and altered monzonitic rocks in the Bingham Mining District, Utah.* Economic Geology, 68, 269-280.

Munoz, J.L., 1984. *F-OH and Cl-OH exchange in micas with applications to hydrothermal ore deposits.* In Bailey, S.W. Ed., Micas, Reviews in Mineralogy 13, 469-494. Mineralogical Society of America, Chantilly, Virginia.

Nachit, H., Ibhi, A., Abia, El Hassan, Ben, Ohoud Mohcine, 2005. *Discrimination between primary magmatic biotites, reequilibrated biotites, and neoformed biotites.* Comptes Rendus Geoscience, Vol. 337, No.16, 1415–1420.

Nagornaya, E.V., 2013. *Mineralogy and zoning of porphyry copper-molybdenum field Nakhodka, Chukchi Peninsula.* Candidate Dissertation, Moscow State University, Moscow, (in Russian).

Parry, W.T., Jasumback, M., 2002. *Clay mineralogy of phyllic and intermediate argillic alteration at Bingham, Utah.* Economic Geology, 97, 2, 221–239.

Pécskay, Z., Edelstein, O., Kovacs, M., Bernard, A., & Crihan, M., 1994. *K/Ar age determination of Neogene volcanic rocks from the Gutîi Mts. (Eastern Carpathian, Romania),* Geologica Carpathica, Vol. 45, No. 6, 357-363.

Pécskay, Z., Edelstein, O., Seghedi, I., Szakács, A., Kovacs, M., Crihan, M., Bernad, A., 1995. K-Ar datings of the Neogene–Quaternary calc-alkaline volcanic rocks in Romania. Acta Vulcanologica 7, 53– 63

Pirajno, Franco, 1992. *Hydrothermal Mineral deposit. Principles and Fundamental Concepts for the Exploration Geologist.* Springer-Verlag Berlin, Heidelberg, New York, London, Paris, Tokyo, Hong Kong, Barcelona, Budapest, pages 709.

Plotinskaya, O. Yu., Damian, F., Prokofiev, V. Yu. Kovalenker, V. A. & Damian, Gh., 2009. *Tellurides occurrences in the Baia Mare region, Baia Mare.* Carpathian Journal of Earth and Environmental Sciences, Vol. 4, No. 2, 89 -100.

Rogacheva, Lyuba & Baksheev, Ivan, 2010. *Mineralogy of metasomatic rocks and geochronology of the Olhovka porphyry-copper deposit, Chukotka, Rusia*. Geophysical Research, Abstracts Vol., 12, EGU, pp. 556.

Seghedi, Ioan, Downes, Hilary, Szakács, Alexandru, Mason, Paul R. D., Thirlwall, Matthew F., Roşu,

Emilian, Pécskay, Zoltán, Márton, Emö & Panaiotu, Cristian, 2004. *Neogene-Quaternary magmatism and geodynamics in the Carpathian-Pannonian region: a synthesis.* Lithos, Vol. 72, No. 3-4, 117-146.

Seghedi, Ioan, Downes, Hilary, Harangi, Szabolcs, Mason, Paul R.D. & Pécskay, Zoltán, 2005. Geochemical response of magmas to Neogene–Quaternary continental collision in the Carpathian Pannonian region: A review, Tectonophysics 410, pp.485–499.

Selby, D. & Nesbitt, B.E., 2000. *Chemical composition of bitote from Casino porphyry Cu-Au-Mo mineralization, Yukon, Canada: evaluation of magmatic and hydrothermal fluid chemistry.* Chemical Geology, 171, 77–93.

Sillitoe, R. H. & Hedenquist, J.W., 2003. *Linkages between volcanotectonic settings, ore-fluid compositions, and epithermal precious metal deposits.* Society of Economic Geologists Special Publication, 10, 315-343.

Skuridin, V.A., 1984. *Chemical features of biotites from rocks of ore-bearing stocks at Cu-Mo occurrences in Western Transbaikal region.* In: Tr. Institute of Geology and Geophysics, Siberian Branch, Russian Academy of Sciences, 587, 53-69 (in Russian).

Sotnikov, V.I., Berzina, A.T. & Berzina, A.P., 2002. *Fluorine on light micas of Siberian and Mongolian porphyry copper-molybdenum deposits and its probable origin*. Geochemistry International, 40, 10, 1004-1012.

Voudouris, Panagiotis C. 2014. *Hydrothermal corundum, topaz, diaspore, and alunite supergroup minerals in the advanced argillic alteration lithocap of the Kassiteres-Sapes porphyry-epithermal system, western Thrace, Greece.* Neues Jahrbuch für Mineralogie, Abhandlungen: Journal of Mineralogy and Geochemistry, Vol. 191, No. 2, 117–136.

Yang, K. & Jang, J.-Y. 2002. *Geochemistry of tourmalines in the Ilgwang Cu–W breccia-pipe deposit, southeastern Gyeongsang Basin.* J. Petrol. Soc. Korea 11 (3–4), 259–270.

Yavuz, F., Iskenderglu, A., Jiang, S.Y. 1999. *Tourmaline compositions from the Salikvan porphyry Cu-Mo deposit and vicinity*. Canadian Mineralogist, 37, 1007–1024.

Received at: 07. 03. 2015
Revised at: 14. 06. 2016
Accepted for publication at: 17. 06. 2016
Published online at: 23. 06. 2016